Materials Advances

ROYAL SOCIETY OF CHEMISTRY

PAPER

View Article Online
View Journal



Cite this: DOI: 10.1039/d5ma01460c

# The influence of rheology on 3D printing with heterogeneous reactive polyurethane reagents

Yuyang Wu,[a] Zuoxin Zhou,[a] Xuesong Lu,[a] Amy Stimpson,[a] Agustin Forchetti Casarino,[ac] Wayne Hayes,[b] Christopher Tuck,[a] Ricky D. Wildman*[a] and Derek Irvine*[a]

The successful printing of multi-layer, multi-material polyurethane woodpile structures with good structural fidelity and rigidity was demonstrated *via* polymerisation-based reactive extrusion processing. Two heterogeneous, viscoelastic feed-streams, *i.e.* a diol and a polymeric isocyanate reagent (which was selected to improve flow-process safety), which contained fumed silica microparticle reagents were mixed and the printing performance was shown to be governed by relative rheological properties of the feeds and by the polymerisation exotherms generated upon mixing. The influence of the polymer rheological characteristics on the polymerisation, exotherms and extent of reaction achieved has not been extensively explored to date. To understand the impact of feedstock characteristics on the printing process, polydimethylsiloxane coated fumed silica particles were added to the two polymer feeds. These were designed to act as: (a) inorganic functional materials to modify the material properties of the printed devices, (b) additives that modify the feed materials' rheology and (c) inorganic fillers that moderate the polymerization exotherm. The experimental results demonstrated that the viscosity and elasticity of the poly(isocyanate) feed, which is tuned through silica particle content, must be comparable to or lower than those of the diol feed. This requirement was attributed to the mixing characteristics that developed when the two feed streams were combined, which ultimately determined the interfacial reactive area created and dictated the rate/extent of the step-growth reaction.

Received 13th December 2025,
Accepted 24th April 2026

DOI: 10.1039/d5ma01460c

rsc.li/materials-advances



## Introduction

Additive manufacturing (AM), or 3D printing, is a broad descriptor for a range of techniques that build structures layer by layer *via* translation from 3D computer-aided design (CAD) models.[1,2] AM techniques offer significant advantages in fabricating complex, personalized and multi-functional structures when compared with conventional manufacturing methods. Meanwhile, polyurethane (PU) polymers are one of the most versatile materials currently in commercial use. They combine rubbery and rigid plasticity domains within their structure,[3,4] and their mechanical properties can be tuned by modifying the chemical structure of the hard and soft segments. This characteristic has allowed the development of a great number of applications in different end-uses, *e.g.*, foams,[5] coatings,[6] adhesives,[7] and biomedical devices.[8]

AM has shown great potential for enabling increased flexibility in the fabrication of PU products. To date, the use of PU materials in AM has centred on the application of commercially available synthesized powders or resins as feedstocks for various AM techniques, such as powder bed fusion, material extrusion, and vat photo-polymerization.[2,9–11] Thermoplastic PUs (TPUs) have been processed through powder bed fusion or material extrusion to fabricate designed, flexible, auxetic lattice/cellular structures for use in energy absorption and mechanical damping applications.[11,12] Biomedical TPU implants with tuneable drug release rates have also been fabricated *via* paste extrusion using pre-synthesized thermo-responsive supramolecular PU.[8] However, using a pre-synthesized PU feedstock for fabrication also limits the capability of selectively tailoring the material properties.

An alternative approach to processing PU is to adopt a reactive process. For example, Reactive Ink-Jetting has been employed to fabricate PU or poly(dimethyl siloxane) (PDMS) *via* an *in situ* reaction at the point of application of two feed materials, without "pre-mixing" of the ink components prior to printing.[13–15] However, typically a solvent was required to lower the ink viscosity, which could result in structural shrinkage and/or restrict the number/type of materials that could be used

[a] *Centre for Additive Manufacturing, Faculty of Engineering, University of Nottingham, UK. E-mail: derek.irvine@nottingham.ac.uk, ricky.wildman@nottingham.ac.uk*
[b] *Department of Chemistry, University of Reading, Whiteknights, Reading, RG6 6AD, UK*
[c] *Added Scientific Ltd, Nottingham Science Park, Nottingham, NG7 2RH, UK*

as inks.[13,14,16,17] A second AM strategy to process PU is Reactive Extrusion (REX), similar in many ''operational'' processing aspects to Direct Ink Writing (DIW), but involves an *in situ* reaction that takes place within a mixed and extruded reagent stream (typically referred to as a bead) during the process of forming a 3D structure.[16] By employing this technique, devices have been produced *via* an in-line mixer and a two-component curing PU system.[18–22] REX involves two feeds of inter-reactive materials being mixed so that they start to react and/or cross-link upon deposition.[23] It has been reported to deliver (a) improved interlayer adhesion through the creation of *in situ* interlayer cross-linking, (b) reduced thermal distortion during printing and (c) high printing speed by capitalizing on fast reaction kinetics.[24] Furthermore, the product properties could be tailored by varying the relative ratio of the two reactive inks. For example, REX printed formulations exhibited higher work-to-failure properties when compared to analogous cast samples in which non-linear mechanical gradients were introduced into TPU structures.[14,17,24]

While many regard DIW as a mature technique from the standpoint of ink development, it is still the most popular 3DP platform for developing novel materials (*e.g.*, resin compositions).[25] Furthermore, adopting *in situ* polymerization in REX means that the success of REX processing requires understanding of the ink's rheological properties to achieve efficient/homogenous mixing and therefore controlled and consistent reaction kinetics, areas where there is still significant scope for investigation.[14,16,24,25] For example, two viscoelastic fluids upon mixing can show different mixing regimes (modes) due to the difference of viscosity and elastic moduli between two fluids.[26] Thus, these different mixing modes will critically influence the degree of polymerisation and final polymer molecular structures produced. The link between these traits and the printability is just beginning to be established for unfilled systems (*i.e.* those that do not contain formulation components that are particulate).[27,28] For those interested in producing ''composite'' materials, the presence of heterogeneous component(s) will also have an influence on the final material properties of the printed structure. Studies on the specific influence of feed heterogeneity have only been reported in the last 5 years or so.[29–31] This is important because for REX to become a more heavily exploited process, a more systematic understanding of the link between the feed material's rheological properties and the final product's material properties needs to be gained. Only then will it be possible to reliably program target behaviour into final products *via* the combined choice of reagent materials and designed depositions.

This study reports a polymer chemistry focused investigation of bead production, which attempted to relate observations on the reaction exotherms exhibited by various feed formulations to the rate and extent of reaction achieved. Furthermore, isocyanates are typically irritants and respiratory sensitisers and so the use of relatively low molecular weight isocyanates, such as the industrially applied toluene di-isocyanate (TDI), can lead to hazards as its vapour can be inhaled.[32,33] Consequently, PU manufacturing is often performed *via* batch processing to circumvent the issue with handling of the isocyanate, because this allows the vessels/apparatus to be sealed or located in isolated buildings in case isocyanate vapour is released during the heating process or due to the reaction exotherm.[34] As a result, achieving safe *in situ*, flow manufacturing strategies, such as REX, can potentially be challenging with PUs. Thus, this work was not intended to be an in-depth study of the influence of the formulation viscosity on overall REX manufacture. Rather, it aimed to define how feed viscosity influences the level/modes of feed mixing that was realised and hence the extent of reaction that was achieved, and also to investigate the use of a polymeric isocyanate in flow processing, because it has a much lower toxicological footprint due to its very low volatility. The resulting conclusions were then tested by observing the print and material/rheological characterization to confirm the differences in the polymer/bead produced.

In practice, no toxicological evaluation was conducted as part of this study, rather this view was built on the findings of a 2014 review of the use of isocyanates.[35] This concluded that the route forward to reduce exposure and risk from PU chemistry was to continue the search for ways to substitute TDI with the three orders of magnitude less volatile MDI, including taking this forward to the adoption of the even less volatile modified/pre-polymerised MDIs.[35] Furthermore, the authors did highlight that the potential for further substitution in this vein was generally receiving low levels of interest due to the highly reactive product needed in the end-use application. To this end, they identified the use of modified/pre-polymerised MDIs as one of the key gaps for future development in this area as these are less toxic than monomeric MDIs.[35]

To do this, a range of heterogeneous, multi-material feed formulations containing either a polymeric isocyanate or a multiple hydroxyl group containing reagent were developed, both of which contain an additional functional inorganic material in particulate form. Furthermore, one of the key objectives of this study was to explore the synthesis of polyurea with higher molecular weight polymeric isocyanate. Therefore, poly[(phenyl isocyanate)-*co*-formaldehyde] (PMDI), a polymeric isocyanate of 3 to 4 repeat units (thus multiple isocyanate groups) was used,[36] because its lower volatility enabled it to be applied in the REX apparatus with only local, bench top extraction. Fig. S1 contains the general molecular structure of PMDI and the diols used, *i.e.*, 1,4-butandiol (1,4 BD) and poly(ethylene glycol)-*b*-poly(propyleneglycol)-*b*-poly(ethylene glycol) (PEG–PPG–PEG). The significance of these properties on the mixing, reaction kinetics and thermo-mechanical properties of REX-produced cross-linked thermoset PU inorganic–organic composite materials by using a multi-functional group poly(isocyanate) is discussed. To achieve this, poly(dimethylsiloxane) (PDMS) coated fumed silica (FS) particles were introduced into the feeds to act as both rheology modifiers and exotherm suppressants. This strategy was adopted because there was a desire to include functional additives into 3D printed articles to deliver end-use effects and subsequently a concern that excessive temperatures in the printed bead will also influence the material properties. Studying the properties of the printed multi-material structures enabled us to propose

the type of process mixing achieved and address a key gap in the current REX research field.

## Materials and methods

### Materials

The PU materials were synthesized from the following polyols and poly(isocyanate). Poly[(phenyl isocyanate)-*co*-formaldehyde] (PMDI, average $M_n$ = 340), poly(ethylene glycol)-*b*-poly(propylene glycol)-*b*-poly(ethylene glycol) (PEG-PPG-PEG, average $M_n$ = 1900), 1,4-butanediol (1,4 BD, ReagentPlus®, 99%), and dibutyltin dilaurate (DBTDL, 95%) were purchased from Sigma Aldrich. Polydimethylsiloxane (PDMS)-coated hydrophobic fumed silica particles (Cabosil TS720, Cabot Corporation, United States) were used as the rheology modifier. All chemicals were used as received without further purification.

Note: all numerical values reported in the manuscript are derived from replicated experiments ($n \geq 3$) conducted during the project. Thus, the printing focused datasets presented were generated from multiple experiments using consistent experimental conditions and it was observed that the trends in structure–property relationships reported here were consistent from experiment to experiment, reflecting the consistent differences arising from formulation chemistry, feed rheology, and mixing mode observed under controlled conditions. However, the REX processing variability meant that the process variation had greater influence than the chemistry induced errors. Thus, the approach taken in this manuscript was to report one set of experimental data rather than averages to reflect the effects of chemistry on the process. This aligns with practice in process-driven AM research, where reproducibility and deviation from design intent/practice are often of greater practical significance than statistical variance. Therefore, to reflect this strategy and to simplify the data presentation, the estimated process-induced deviation between individual experiments for the various measurements was added to the titles of the relevant tables in the main manuscript.

### Synthesis and processing

**Feed preparation.** Prior to being introduced to the REX apparatus, each reagent mixture was pre-mixed using a Dual Axial Centrifugal mixing unit (DAC 400 mixer, SpeedMixer™) to prepare the separate isocyanate and polyol feedstock. Robust mixing was conducted at 2200 rpm for 20 minutes so that a homogenous mixture between the reagents and the additives was achieved. Fumed silica (FS) was the additive introduced to modify the rheology and improve the printability of the feedstocks.[37–41] By mixing the isocyanate (NCO) feed with different FS loadings, this part of the system could be designed to exhibit different rheological characteristics (see Table S1 in the SI). From the data generated during this study, it was proposed that there were three different reagent feed stream conditions that would lead to different mixing modes (MM) being established using this strategy. These MM feed scenarios were designated as MM1, MM2 and MM3. It was proposed that in MM1 type mixing the NCO feed was regarded as the dispersed phase and the OH feed as the continuous phase, so forming droplets of NCO in the continuous OH stream after mixing. If the two feeds exhibited similar rheological properties it was referred to as MM2 type where both the NCO feed and OH feed were proposed to be the continuous phases likely to form laminar mixing structures. The third is a less viscous NCO feed when compared to the OH feed and was identified as MM3, in which the OH feed was taken to be the dispersed phase and the NCO feed the continuous one, so potentially forming droplets of OH in the NCO continuous stream post mixing. The FS loadings in the isocyanates feed used to achieve these modes were 5, 2.5, and 1 wt% from MM1 to MM3, respectively, whilst the FS loading in the polyol (OH) feed was kept constant at 5 wt%. The molar ratio between isocyanates and polyol was fixed at 1.15 : 1 (NCO : OH) to minimize additional side reactions with both entrained and atmospheric moisture.

To ensure consistency in results, purchased samples of the PMDI were obtained in small unit sizes to prevent unreacted reagent aging. Once opened, these were stored in a vacuum desiccator to reduce the long-term exposure of the material to atmospheric moisture. Sample transference and apparatus preparation was conducted under an inert atmosphere to ensure that all sample exposure to moisture was consistent. The poly(isocyanate) reagent sampling was conducted immediately before use each time a print was performed.

**Reactive extrusion.** Following feedstock preparation, a REX system was used to co-extrude isocyanate and polyol feeds to react and print PU structures (see Fig. S1 for diagrammatical representation of mixing head design and proposed chemistry). The system was modified from a LulzBot TAZ6 printer (FAME 3D, Fargo, North Dakota, USA) to integrate with a high precision volumetric dosing unit (Preeflow eco-DUO450 two-component mixing dispenser, ViscoTec) (see Fig. S2). Both isocyanate and polyol feeds were transferred into 360 mL Optimum® syringe barrels (Nordson EFD). Subsequently, a lab-built feed supplying system pneumatically transported the reagent mixtures from Optimum® syringe barrels to the dosing unit by pressurized nitrogen, at 3 bar. Feeds from both sides were then driven by a screw pump inside the dosing unit (Fig. 1). The mixing ratio and the flow rate were regulated using a control box (Preeflow eco-Control EC200-DUO). The NCO and OH feeds (Table S1) were mixed at a ratio of 1 : 1 v : v, (or 1.15 : 1 (mol : mol)) in the static mixer (IDMMKH03-16S, Intertronics) (outlet internal diameter (ID) = 1 mm, inlet ID = 3.2 mm, length ($L$)/diameter ($D$) = 23, the number of mixing elements = 16, see Fig. S2), and extruded onto the print bed. An initial study found that the ideal flowrate was 2 mL min$^{-1}$, as the bead was deposited consistently without clogging in the mixer. To demonstrate the printability of the formulations: (a) woodpile structures (4 layers, 21 mm × 21 mm) and (b) bar samples (2 layers, 80 mm × 4 mm) were printed using feeds which exhibited the characteristics of each of the three separate MMs. The bar samples were later used for thermo-mechanical characterization.

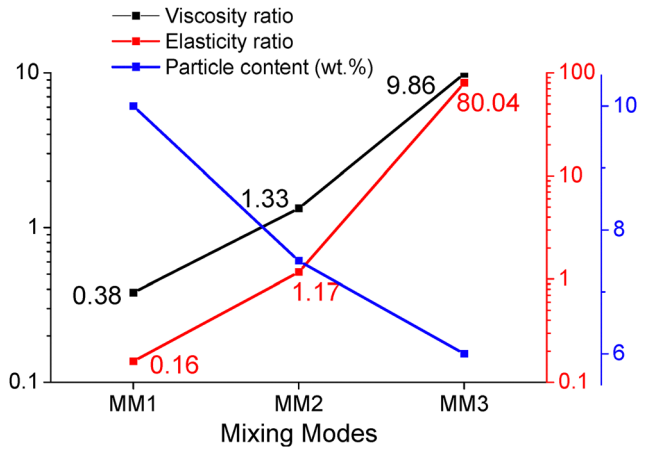


Fig. 1 Plot of the viscosity ratio ($\eta_{OH}$:$\eta_{NCO}$), elasticity ratio ($G'_{OH}$:$G'_{NCO}$) and particle content loadings that result in the three MMs.

## Characterization

**Rheology measurements.** The dynamic rheological properties of the NCO and OH feeds (Table S1) were measured by the Kinexus Pro+ rheometer (Malvern Instruments) equipped with a 40 mm parallel plate geometry. The apparent viscosity and shear stress were recorded as a function of shear rate ranging from 1 $s^{-1}$ to 100 $s^{-1}$, at 25 °C. Amplitude sweeps were performed to determine the linear viscoelastic region, automatically calculated by the software (Malvern rSpace). Subsequently, frequency sweeps were carried out to determine the viscoelastic profile of the feeds at frequencies from 10 to 0.1 Hz with a fixed 1% shear strain within the pre-determined linear viscoelastic region at 25 °C. The gap between the parallel plates was set at 1 mm. Oscillatory stress ramp tests were run to reveal the yield stress of the investigated NCO and OH feeds. In this test, feeds were subjected to an increasing shear stress from 0.01 Pa to 1000 Pa. The yield stress was determined at the cross-over point between $G'$ and $G''$ data under stress-controlled oscillatory measurements.[19] In this study, two parameters were defined to compare the rheology properties between NCO and OH feeds. The viscosity ratio ($\eta_{OH}/\eta_{NCO}$) was calculated by determining the viscosity of OH and NCO inks at a shear rate of 20 $s^{-1}$, which corresponds to the shear rate at the inlet of the static mixer. The elasticity ratio $\left(G'_{OH}/G'_{NCO}\right)$ is determined at a frequency of 2 Hz.

From a literature study it was defined that static mixer shear rates for REX systems typically fall within the range of ~2 and ~61 $s^{-1}$ depending on nozzle geometry and flowrate.[42] Thus, the chosen shear rate of 20 $s^{-1}$ lies well within that operational envelope. Similarly, it has been reported that fluids experience repeated deformation events each time they pass a mixing element and the characteristic deformation timescale corresponds to approximately 1–3 Hz.[43] A frequency of 2 Hz therefore represents the midpoint of this range, providing a meaningful rheological reference point for comparing the elasticity of the two feeds under conditions relevant to the actual mixing environment.

**Fourier-transform infrared spectroscopy (FTIR).** FTIR was used to investigate the conversion to PU *via* reaction between isocyanate and polyol feeds for each of the three MMs (MM1, MM2 and MM3). A Frontier (PerkinElmer) spectrometer was used. PU samples printed from the three MMs were tested using the spectrometer immediately following extrusion from the static mixer. The spectra were recorded from 4000 to 600 $cm^{-1}$, with a resolution of 4 $cm^{-1}$. The analysis was performed using the PerkinElmer Spectrum software by evaluating the normalized peak areas to determine the reaction conversion. The normalisation to the C–H peak was performed after verifying that the C–H stretching region showed no detectable peak area change across all timepoints, confirming its appropriateness as an internal standard. The revised manuscript therefore clearly identifies each processing step and clarifies the assumptions underlying the conversion estimation. The PU conversion was monitored by following the disappearance of the isocyanate (NCO) absorbance band in the region 2350 to 2100 $cm^{-1}$, and with an absorbance band at 2250 $cm^{-1}$.[44–46] The reference alkane (C–H stretch) peak remained unchanged. Hence, conversion was calculated by comparing the printed ratio of the NCO absorbance band (2350 to 2100 $cm^{-1}$) relative to that of the unchanged C–H stretch absorbance band (~2960 $cm^{-1}$) to the initial isocyanate and alkane peak ratio, using eqn (S1) in the SI.[13,44]

**Reaction exotherm measurement.** The reaction exotherm for different MMs was monitored by using K-type thermocouples (RS PRO), together with a Picolog data recorder. Printed sample temperatures were captured every second by the apparatus continuously for 60 seconds.

**Thermogravimetric analysis (TGA).** TGA was carried out on a PerkinElmer Thermogravimetry Analysis 4000 apparatus to analyse the thermal stability of the printed PU samples. Specimens of approx. 10 mg were sectioned from the printed samples. They were heated from 50 to 800 °C at a heating rate of 20 °C $min^{-1}$ under a nitrogen atmosphere.

**Differential scanning calorimetry (DSC).** DSC was conducted using a PerkinElmer DSC 8000 to study the phase transition temperature of the printed PU samples. Samples of ~10 mg were sectioned from the printed samples and subjected to a heat/cool/heat experiment. In the first stage, the sample was heated from ambient temperature to 150 °C. After that, in a second stage, the sample was cooled down to −50 °C. Subsequently, the material was taken through a second −50 to 150 °C heating cycle at a heating rate of 5 °C $min^{-1}$ under a nitrogen environment.

**Dynamic mechanical analysis (DMA).** The thermomechanical properties of printed PU samples were assessed using a PerkinElmer DMA 8000. Tension geometry was deployed to perform the analysis. Specimens of 10 mm (length), 4 mm (width) and 2 mm (thickness) were sectioned from the printed samples. The specimens were subjected to sinusoidal forces within the linear viscoelastic regions under a constant frequency (1 Hz), isothermally at 25 °C for the first three minutes, then through a temperature scan from 25 to 150 °C at a 5 °C $min^{-1}$ heating rate, and finally by being held at 150 °C for three minutes.

## Results and discussion

### Feed material and product PU rheology, reactivity and material property analysis

In REX 3D printing, the mixing efficiency and reaction kinetics are both highly interconnected and greatly influenced by the relative rheology of the two reactive reagent feed streams.[47] Ultimately, the mixing and level of interstream reaction achieved will greatly influence the properties of the final AM produced PU materials, so, it is important to understand this link between mixing and product performance. The morphologies achieved when mixing viscoelastic fluids, such as those used in REX feed streams, have been studied extensively, and it has been reported in the literature that one of following morphology types will form: matrix/droplet,[48] matrix/fiber,[49] or co-continuous.[50] Furthermore, as highlighted in the Introduction section, when viscoelastic fluids have been mixed through a static mixer, a further morphology type, defined as a dispersed droplet/continuous phase, could be formed under the correct conditions.[26,51]

In the REX-based PU processing conducted in this study, the following feeds are in contact within the static mixer. Feed 1, designated as the OH feed, was a mixture of a polymeric diol soft segment and a low molecular weight reactive diol (1,4-butanediol). Feed 2, the NCO feed, was an isocyanate feed composed of a polymeric isocyanate. The reactive formulation was completed by the inclusion of a polymerization catalyst (dibutyltin dilaurate (DBTDL), 1 wt%). Thus, it was proposed that the main characteristics of the two reagent feed streams which would most effect the mixing achieved were the relative viscosities and elasticities of the polymeric reagents that they contained.[52] Therefore, these characteristics could potentially be used to manipulate, and significantly differentiate, the mixing behaviours (or modes) exhibited by the product bead produced when the individual feed streams were brought together. The hypothesis was that, when the two viscoelastic feeds are in contact within the REX static mixer, domain segregation/formation would occur, as has been reported previously in the interfacial polymerization found in PU chemistry.[53–55] In this case, the form of the domains would be very likely to be highly dependent on the relative feed viscosities and elasticity of the polymers.[52] Therefore, an interfacial reaction zone would be generated between the dispersed and the continuous phases where the polymerization would take place. Thus, the rheological properties would effectively determine the reaction rate, by defining the relative inter-reagent surface areas and diffusion limitations created between the two reactive reagents.

Thus, the effect of adding FS particles upon the feed formulation's rheological properties (*i.e.* viscosity and elasticity $G'$) was examined to generate empirical data that could support the MM hypothesis defined above. Developing this understanding would lead to the development of a link between processing conditions and final PU bead properties.

Additionally, the addition of silica particles/nanoparticles can also beneficially affect other material properties. Silica particles exhibit high rigidity and, with the correct coating applied for a specific polymer matrix, can exhibit excellent bonding characteristics. This, in turn, can strengthen the material by inhibiting crack propagation and improving resistance to mechanical stress. However, including too high a loading can lead to poor particle dispersion which causes agglomeration, creating weak regions that serve as failure initiation sites. Thus, there is typically a balance between strength and flexibility in particle-reinforced composites as a result.[56] Furthermore, the thermal stability of polymer composites is mainly tested by means of thermogravimetric analysis. Taking polymethyl methacrylate (PMMA) as an example matrix polymer, better thermal stability was reported by Wang *et al.* when they added silica/zirconia or silica/titania particles to PMMA, which led to the formation of an organic–inorganic network where composites were prepared *via in situ* polymerization.[57,58] A second thermal benefit is also demonstrated in this study, where their inclusion acts as a thermal sink to reduce the polymerisation exotherm that was observed.

Furthermore, with respect to the rheological effect of adding silica particles, it has also been reported that the feed rheological properties are also key indicators of whether the feed mixture can be self-supporting when deposited onto the print bed as a bead.[59] Hence, FS were added to the feeds in varying quantities to produce three different relative rheology feed combinations. In practice, the OH feed was kept with a fixed FS level, whilst the FS amount in the NCO deed was varied to change its rheological characteristics. So, to generate different MMs during processing, the following feed combinations were found to deliver the target relative OH:NCO feed viscosities: (a) an NCO feed with a viscosity ($\eta$) and elasticity $G' >$ the OH feed, defined as the Mixing Mode 1 (MMI) type feed combination, which needed a feed formulation which comprised of NCO + 5% $SiO_2$ and OH + 5% $SiO_2$, respectively, (b) an NCO feed with $\eta$ and $G'$ values $\cong$ to that of the OH feed (MM2 type) requiring feeds comprising of NCO + 2.5% $SiO_2$ and OH + 5% $SiO_2$ and (c) MM3 behaviour was defined as the combination of an NCO feed with $\eta$ and $G'$ values « than the OH feed for which NCO + 1% $SiO_2$ and OH + 5% $SiO_2$ feeds were required. Plots of the viscosity against shear rate and storage modulus *versus* frequency for all four feed formulations are compared in Fig. S3(a) and (b) in the SI. Meanwhile, the key comparisons that were proposed to have an influence over the domain conformations upon mixing in the REX system are shown in Fig. 1.

This data confirmed that the incorporation of FS particles into the feed influenced their rheological properties and achieved the desired rheological property differences in the feed streams to generate the desired MM types. Hence, to understand the potential influence that this would have upon processing, the effect that adding FS particles had upon the rheological properties of both the isocyanate and polyol feeds was examined in greater detail to compare the relative changes in: (a) $\eta$ as a function of shear rate and (b) change in dynamic moduli as a function of frequency. The data for both feeds (Fig. 2 = NCO feed and Fig. S4 = OH data) showed: (a) shear thinning behaviour (*i.e.*, a reduction in viscosity with increasing shear rate) with all the feed mixtures that contained FS, whilst

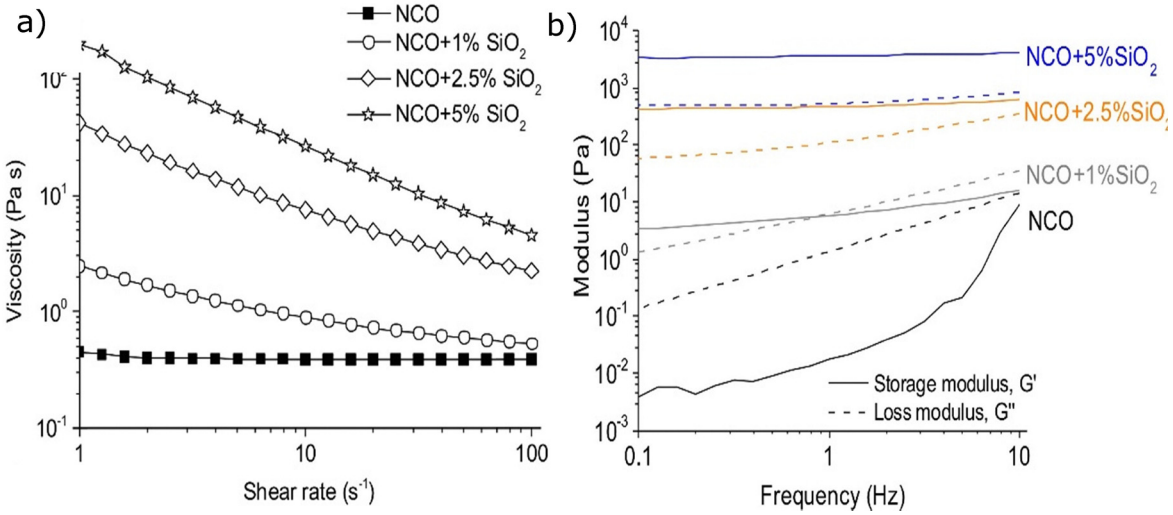


Fig. 2 Plots of viscosity as a function of shear rate and both storage and loss moduli as a function of frequency for NCO feeds.

the neat reagents exhibited apparent viscosity values that were independent of shear rate and (b) viscosity increased as FS content increased.

In the case of the NCO feed, the addition of 1% FS produced a ''crossover'' in the $G'$ and loss modulus ($G''$) values (*i.e.*, $G''$ began to exhibit larger values) at 1 Hz. This kind of crossover is typically taken to indicate where the feed starts to exhibit viscoelastic solid-like behaviour. At higher FS loadings, both the $G'$ and $G''$ increased with the further addition of silica particles, but the independent crossover point was not reached over the full range of frequencies tested indicting that both NCO + 5% FS and NCO + 2.5% FS exhibited more elastic solid behaviour (Fig. 2b). For the polyol feed material, OH + 1% FS behaved as a viscous liquid, with lower $G'$ and $G''$ over all the frequencies tested. However, consistent with the isocyanate feed mixtures, the feeds OH + 5% FS and OH + 2.5% FS both exhibited elastic-like solid behaviour. Typically, both the $G'$ and $G''$ values of the 100% reagent samples were lower than the samples containing the silica particle loadings and the neat reagent $G'$ values were also noted to be dependent on frequency. The inflections in the neat sample data were attributed to thermal artifacts due to the higher exotherms observed, as they contained no filler to moderate the temperature. This was supported by the lack of inflections in the FS samples, where filler was present.

Thus, it was concluded that both the NCO and OH feeds with higher FS loadings exhibited material properties that literature reports would suggest are suitable for AM processing, as these material characteristics are essential in preventing distortion during printing processes.[16,29,31] Consequently, the addition of FS to the feeds resulted in a change from Newtonian to non-Newtonian behaviour, *i.e.*, the viscosity of the neat reagent mixtures was independent of the shear rate but those of the FS-containing feeds were dependent on this parameter. This was attributed to the formation of an inter-particle percolation network within the polymer matrix,[16,60,61] created by associative interactions between the particles. For example, this may result from interactions between the polar groups within the PDMS coatings on the FS particles' surface.[62] The percolation network concept is linked to processes where a liquid must pass through a porous media, *e.g.* grease formation.[63,64] In this case, it was proposed that the interactions between particles that are in mutual contact create the ''porous aggregates'', through/around which the reagents must pass in order to flow around the system. As such, a percolation threshold must be reached, such that sufficient long-range connectivity is achieved between the particles, to influence the flow behaviour of the media. Below the threshold an extended connected network does not exist.[63,64]

This conclusion was supported by the observation that only the FS-containing feeds exhibited shear thinning behaviour (Fig. 2a and b), and by the fact that the inclusion of particles in different concentrations has previously been observed to change shear behaviour.[65] This was proposed to result from the disassociation and slower reformation of the percolated network when the applied shear forces were increased. Thus, the introduction of FS particles as formulation additives was highly desirable due to their capacity to both absorb part of the heat generated during polymerization (exotherm management) and act as shear thinning agents for the feeds which allows extrusion-based 3D printing without the need for excessive pressure (viscosity management).[16,41]

The effect of introducing FS into the feed on the material's yield stress was also investigated, and these results are shown in Fig. 3a and b.

This data showed that both the neat feeds and those with 1% FS loading behaved as viscous liquids, *i.e.*, the $G''$ value was found to be higher than the $G'$ value regardless of the shear stress applied. By comparison, formulations with 2.5% and 5% FS exhibited elastic solid behaviour when subjected to low shear stress. Additionally, the $G'$ and $G''$ data exhibited cross-over points as stress increased. After the cross-over point, they

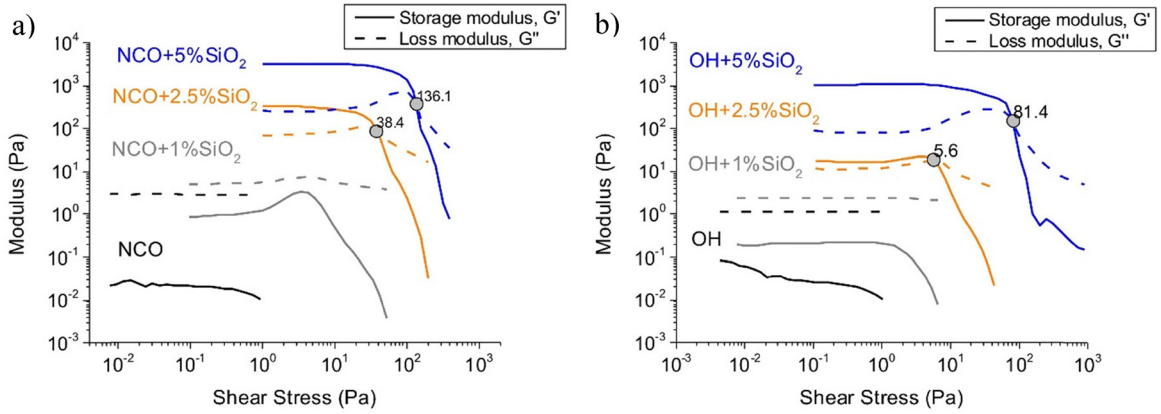


Fig. 3 Oscillatory rheology data of the investigated feeds showing a plot of modulus *versus* shear stress for the (a) isocyanates (NCO) and (b) polyol (OH) feeds.

would be predicted to behave like a viscous liquid *i.e.* the $G''$ value to be higher than the $G'$ value. Furthermore, higher yield stresses were exhibited by the NCO feeds when compared to the OH with same level of FS loading. This was attributed to better interaction/wetting between the FS particles with the NCO matrix materials, which allowed the FS particles to form the percolated network more easily. When compared with neat polymer, the FS filled polymer matrix was then better able to store and dissipate energy when stress is applied, resulting in higher dynamic modulus ($G'$ and $G''$) values. Hence, the substantial increase in yield stress and high $G'$ values exhibited by both 5% FS loaded feeds was considered favourable for extrusion 3D printing, as it should result in the printed structure retaining its fidelity when undergoing multi-layer stacking *i.e.* retention of shape upon both extrusion and when supporting a subsequent layer built on top.[66]

Further experimentation showed that reaction kinetics were also observed to be influenced by the MM achieved. The reaction kinetics of the three MM systems were monitored and compared *via* use of FTIR spectroscopic analysis, and these data are shown in Fig. 4 for the NCO peaks, and Fig. S5 for the C═O peaks (both H-bonded and non-H bonded).

The IR spectroscopic data confirmed that significant cure levels were achieved within the first 10 minutes of processing. In all three MMs, as the PU reaction progressed from 1 to 10 minutes, significant reductions in the characteristic IR absorbance bands for the isocyanate group ($\sim$2250 cm$^{-1}$) were observed in all samples (Fig. 4a). Meanwhile, the C–H absorbance band at $\sim$2865–2968 cm$^{-1}$, which is not involved in the polymerization, was noted to remain unaltered throughout the reaction. Thus, the relative NCO reduction could be ascertained by comparing the areas of these two absorbance bands and used to define the level of monomer consumption. A stretching vibration from either a hydrogen bonded N–H group ($\sim$3300 cm$^{-1}$) or a hydroxyl group resulting from the NCO reaction with entrained/atmospheric water was observed.[44,45,67] The absorbance bands at $\sim$1725 and $\sim$1701 cm$^{-1}$ were attributed to free and hydrogen bonded urethane carbonyl groups.[45,68] Interestingly, a more intense hydrogen-bonded C═O absorbance band in contrast to the free C═O absorbance band was displayed for MM3 (Fig. S5a), compared to the MM2 or MM1 derived PU. This suggested that there was a high level of interchain/segment interaction occurring in the MM3 polymer due to hydrogen

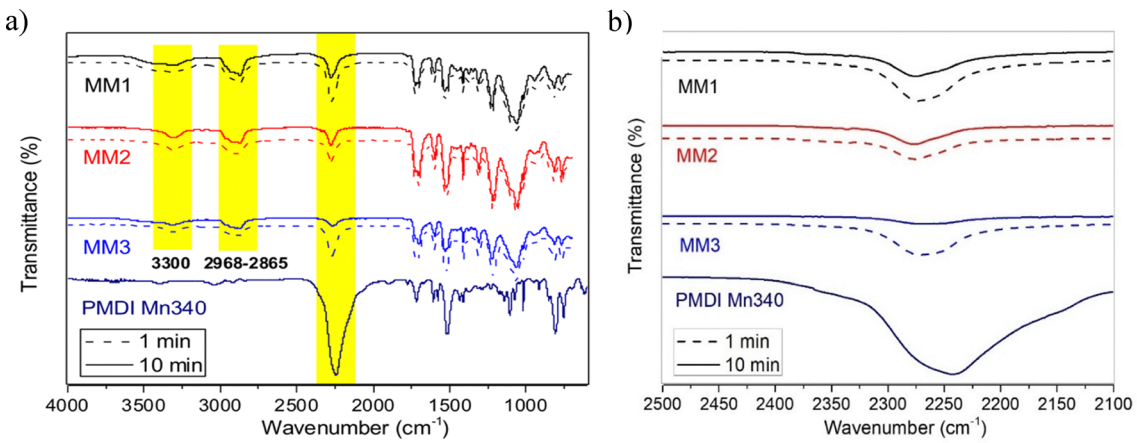


Fig. 4 FTIR spectra of PMDI $M_n$ 340, PU printed from MM1, MM2 and MM3 after printing at 1 minute (dash line) and 10 minutes (solid line). (a) The full spectrum and (b) a blow-up of the isocyanate peak (–NCO) region.

Table 1 Reaction conversion of PU printed utilizing MM1, MM2 and MM3 modes at 1 and 10 minutes, calculated by comparing the relative percentage reduction in the NCO to CH peaks. The estimated process induced deviation between experiments ±4%

| | Reaction conversion (%) | | |
|---|---|---|---|
| Time (min) | MM1 | MM2 | MM3 |
| 1 | 80 | 84 | 83 |
| 10 | 84 | 87 | 93 |

bonding interactions, which would result in an increase in the stiffness of the material. Additionally, the NCO absorbance band for MM3 was noted to be smaller than those of MM1 and MM2 at 10 minutes, potentially indicating higher reaction conversion and faster reaction kinetics exhibited by systems that display MM3 behaviour (see Fig. 4b, Table 1 and Table S2, the latter of which defines the calculation method).

The thermal properties of the printed PUs were also analysed and compared. The TGA thermograms (Fig. 5a) for all three MMs sampled at 10 minutes were very similar, with the exception that MM1 exhibited slighter greater levels of mass loss in the 150–350 °C region.

This increased weight loss was proposed to indicate a combination of: (a) higher levels of low molecular weight oligomers, because of lower levels of cure/cross-linking, as observed in the FTIR data (Fig. 4 and Table 1) and (b) impurities introduced into the system from the surface of silica particles,[68,69] where the former was thought to be the more significant. Consequently, the TGA's of the polymeric reagents, which were available in the literature were compared to this data. Both those of the PMDI[70,71] and polymeric diol,[66] because they are polymeric, did not to exhibit any weight losses below 300 °C, suggesting that they did not contain low molecular weight materials. Meanwhile, there was no readily available literature reference thermogram for 1,4-butanediol. This is because such low molecular weight, volatile diols typically evaporate before they thermally decompose. Thus, the presence of a weight loss below 300 °C in the MM1 sample potentially suggested that some unreacted butanediol or low molecular weight butanediol oligomers remained in the MM1 sample. This would support the conclusion that this is not the optimum mixing mode for this type of processing, because it suggested that less polymerisation occurred in the MM1 process, which was also supported by the FTIR data. However, these conclusions had to be balanced with the observation that the silica particle coating may have also released low molecular weight species that contribute to their TGA data below 300 °C.

Also, two pronounced peaks (DTG(I) and DTG(II)) were observed in the differential thermogravimetric data of all three MMs (Fig. 5b), indicating the potential that microphase-separation had occurred during printing. DTG(I) was typically located in the 340–370 °C region and DTG(II) within the 430–450 °C range. These corresponded to the decomposition of the urethane bond in the hard segment and ether bond in the soft segment, respectively.[72–74] The DTGs also showed a graduation in the data such that there was greater similarity between MM2 and MM3 than with MM1 (Table 2). This suggested that the thermal stability of the printed material is also influenced by the type of MM achieved.

The glass transition temperature ($T_g$) of the PU is predominantly affected by the mobility of the polymer chains. Lower $T_g$ values will be exhibited when the polymer chains have more freedom to move. So, as more urethane bonds were formed in the structure, the free rotation of the long chain polyol will be restricted, so increasing the $T_g$.[75] Thus, DSC analysis of the PU printed samples was conducted (see Fig. S6 and Table 2 for data) and also showed a trend in the $T_g$ data increasing from MM1 to MM3. Additionally, no melting endotherm was detected, indicating the samples are amorphous cross-linked materials.

Thermal monitoring also demonstrated a trend in the temperatures within the printed samples as a result of the exothermic PU reaction,[76] as shown in Table 2 and Fig. S7. The temperature of the printed samples rose rapidly as a consequence of the exothermic PU reaction.[76] The time at which the exothermic reactions commenced was 14 s, 10 s and 8 s for MM1, MM2 and MM3, respectively (see Table S3 for the complete data set of the thermal profile over the first 60 seconds). Furthermore, MM3 was observed to reach the highest peak temperature. Thus, it was concluded that the highest reaction kinetics was exhibited by MM3, suggesting that there had been more intimate mixing of the reagents with

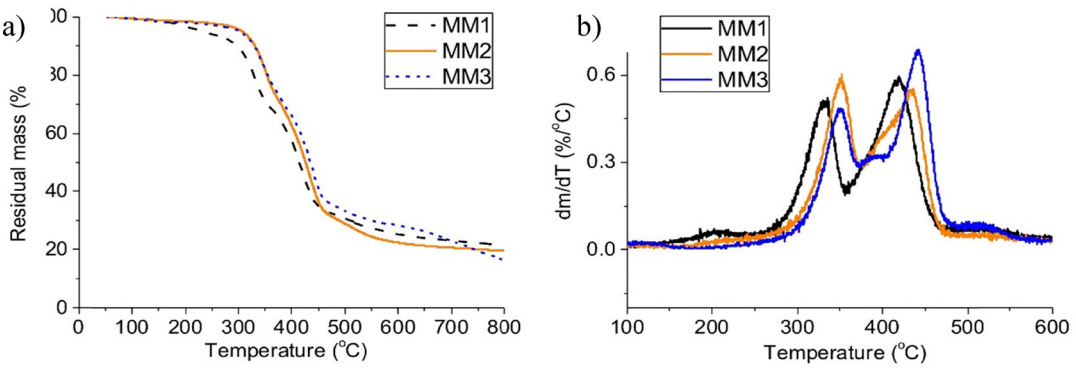


Fig. 5 Plots of (a) TGA mass loss thermograms and (b) differential thermogravimetric (DTG) analysis of PU samples printed from the three MMs.

Table 2 Summary of the thermal properties of PU printed using MM1, MM2 and MM3. $T_{5\%}$ is the temperature at 5% weight loss on the TGA thermogram, DTG(I) and DTG(II) are the lower and higher peak temperatures from the DTG thermogram, $T_g$ is the glass transition temperature *via* DSC and DMA, and $T_1$ and $T_2$ are the sample temperatures at the points in the thermal profile identified as $t_1$ and $t_2$, respectively, where $t_1$ is the start of the temperature increase and $t_2$ is the time when the peak temperature was reached. $\Delta T/\Delta t$ is the rate of change of the sample temperature during the exotherm. $G'$ DMA is the storage modulus measured in the DMA at 25 °C. Estimated process-induced deviation between individual experiments is less than (a) $T_g$ and $T_{5\%} = \pm 4$, (b) DTG = ±9, (c) $T_1$ and $T_2 = \pm 4$ and (d) $G'$ DMA = ±10

| Mode | $T_{5\%}$ (°C) | DTG(I) (°C) | DTG(II) (°C) | $T_g$ DSC (°C) | $T_g$ DMA (°C) | $T_1$ (°C) | $T_2$ (°C) | $t_1$ (s) | $t_2$ (s) | $(\Delta T/\Delta t)$ (°C $s^{-1}$) | $G'$ DMA (MPa) |
|---|---|---|---|---|---|---|---|---|---|---|---|
| MM1 | 252 | 345 | 432 | 51 | 54 | 23 | 36 | 14 | 37 | 0.6 | 142 |
| MM2 | 295 | 362 | 442 | 73 | 61 | 22 | 46 | 10 | 20 | 2.3 | 267 |
| MM3 | 319 | 368 | 451 | 80 | 64 | 19 | 53 | 8 | 16 | 4.2 | 314 |

this mode. Additionally, the rate of reaction exotherm ($\Delta T/\Delta t$) for MM3 was 1.8 times and 7 times higher than the values of MM2 and MM1, respectively. It should be noted that in this chemistry kinetic focussed study no analyses of thixotropy were performed. This strategy was adopted because the structural recovery (thixotropic behaviour) will be complex because an *in situ* reaction is taking place once the feed materials mix. Thus, developing an understanding of the resultant reaction extent/kinetics observed is a key first step in breaking this complex problem down by looking at the indirect chemistry indicators of process performance, Clearly, direct characterisation methods, such as tomography or fluorescence-based imaging, will be needed to form the basis of future studies to present direct validation of these initial conclusions.

The mechanical properties of the three MMs were also assessed *via* dynamic mechanical analysis (DMA), and the variation of the storage modulus and tan delta ($\tan\delta$, *i.e.* the ratio of $G'$ to $G''$) as a function of temperature exhibited by the samples is presented in Table 2 and Fig. S8a and b. The storage modulus of PU from MM3 was found to be higher than that of MM2 and MM1 at 25 °C, again suggesting that the stiffest PU was obtained from MM3. This supported the earlier conclusion that there were greater levels of cross-linking/cure in this sample. All three samples showed single $\tan\delta$ peaks and the temperature at which this peak occurs should correspond to the $T_g$ of the material.[77] The trend in the $\tan\delta$ temperature maxima was an increase from MM1 to MM3, which was the same trend observed with the $T_g$ and was in the same region (45–75 °C) as the DSC recorded data (see Table 2 and Fig. S8b). Furthermore, the actual MM3 $\tan\delta$ value was the highest with the trend increasing through MM2 to MM1. This observation suggested that MM1 exhibited a higher degree of molecular motion, and as a result more energy can be absorbed/dissipated for the MM1 sample, again suggesting that this sample is less crosslinked.

The inferior performance could potentially be mitigated by significantly changing the processing conditions. For example, these effects could potentially be mitigated *via* thermal post-curing. However, in this study, post-curing would not resolve the potential, real-time printing issues, *e.g.* any overhanging structures would have already sagged prior to being able to apply a post-printing thermal treatment. Thus, this was not investigated as part of this programme of work. Additionally, because this was a chemistry focussed study investigating the use of a multi-functional PMDI, the –NCO and –OH group ratio applied was 1.15 : 1, which in theory should ensure the full consumption of the –OH group and yield a high degree of cross-linking, and the results of the MM3 scenario also supported this claim. The fact that the viscosity of both precursors greatly increased in the MM1 scenario was hypothesised to limit the mobility of the molecules and so prevent the functional groups from reacting with each other. Industries which deal with higher viscosity liquid precursors typically apply a monomer molar ratio from 1.5 : 1 to 4 : 1, especially for formulations that contain reinforcement particles/rheology modifiers such as fumed silica, to ensure a high degree of cross-linking. However, the possibility of increasing cross-linking using such ''extreme'' reagent ratio differences was defined to be outside the scope of this initial study due to the multi-functional nature of the PMDI. Rather, its prime focus was to demonstrate that a viscosity which limited the mobility of the molecules would result in the decreased curing speed, less released heat, decreased degree of cross-linking and decreased $G'$ of the final product whilst using a poly(isocyanate) with multiple functional groups.

Thus, from this study, the thermal stability of PUs was concluded to be principally associated with the cure and/or cross-linking density within the structure. Similar hypotheses have also been reported in the literature, where it was proposed that the mobility of soft segments were reduced as a result of the chemical cross-links in the hard segment, and consequently the thermal stability of the polymer was improved.[73,75] Thus, the ascending order of DTG(I) from MM1 to MM3 and the DMA $\tan\delta$ suggests that more cross-linking is achieved with MM2 and MM3. This conclusion is supported by the trend in the reaction's exotherm data, which indicated that the highest level of cure/cross-linking was presented in MM3 samples. This also reinforces the conclusion that MM1 was most affected by diffusion limitations and/or exhibiting a limited reaction interface among the three MMs, whilst MM3 was least influenced.

With respect to REX processing, the stronger cross-linked network formed in MM3 should improve the structure integrity whilst printing. Furthermore, the faster reaction kinetics exhibited with MM3 behaviour could also be beneficial for REX printing, since a higher level of cross-linking could be achieved at a shorter time. Thus, the mechanical results from the DMA analysis supported the FTIR spectroscopic analysis conclusion that more agglomerated hydrogen bonded hard segments are present in MM3, leading to a stronger cross-linked network. This can reduce the free movement of polymers chains, with an

increased $T_g$ and deliver better mechanical integrity from a final bead.

### REX printability analysis

The REX processability of the three formulations was then demonstrated by printing woodpile structures. These are 3D periodic structures showing ''gap spanning/bridging'' features (Fig. 6a),[59,78,79] where the spanning feature is the section of polymer bead in the third layer that bridges the gap between a pair of perpendicular printed beads in layer two. Additionally, the spanning section is also supporting an additional perpendicular bead printed directly above the layer two ''gap'', which provided additional weight on the bridge, as shown in the front view of the printed sample (Fig. 6b).

REX processing was conducted using the standardised parameters to print the MM3 formulation defined in Table S4. These parameters offered consistent bead printing without clogging the mixer. Optical assessment of the printed woodpile structure showed that the printed formulation exhibited good structural integrity. This is defined by the observation that the overhang on the top of the second layer was free-standing (Fig. 6b) and did not bow under the influence of gravity. Thus, the MM3 material bead shows very high levels of resilience, which is even more impressive in this case, as the woodpile was printed such that the spanning structure is also having to support the additional weight of the perpendicular printed bead of layer four.

It also demonstrated high fidelity to the CAD designs (Fig. 6a, c and d). Furthermore, the spatial resolution of the print, which was characterized by estimating the difference of the experimentally achieved block feature size from the values set by the CAD model (Fig. S9 and S10), were found to exhibit $<6\%$ variance in all measurements (see Tables S5 and S6). Overall, the block features showed that the print was of good quality and exhibited good reproducibility, where ''good'' is defined as the woodpile dimensions exhibiting an average deviation of less than 6%. Thus, both of these print features demonstrated that using exotherm feedback from the reaction chemistry allowed us to produce a high-performing bead.

By comparison, MM1 and MM2 woodpile structures were shown to exhibit severe sagging, and loss of structural fidelity was observed. Fig. S11 in the SI file shows the side view of the woodpile prints of MM1 and highlights sagging of the image when this formulation was printed at differing heights. Indeed, at the lower height spacings (*i.e.* 0.5 and 0.75 mm) the gaps in the woodpile structures have closed. This side-by-side comparison directly visualises the practical consequences of sub-optimal feed rheology and mixing mode.

### Data summary and implication

The data from this fundamental study of feed rheology is crucial for the successful design of REX strategies in the future. It has been demonstrated that achieving high quality, free-form, self-sustaining structures, *i.e.* without the need of a support, can be produced *via* REX printing, but only by tuning the feeds to have optimum rheological properties. The hypothesis from this data is that there is an optimum MM behaviour that needs to be achieved upon mixing the feed streams that will deliver the best printing quality. The proposed MM behaviour characteristics, from consideration of the data presented in this study, are shown in Fig. 7.

The hypothesis proposes that in MM1, the viscous NCO feed will tend to segregate into large domains of NCO in a ''flow'' of predominantly OH reagent mixture, because the $\eta$ value of the OH feed will be insufficient to create sufficient shear to produce smaller ''droplets''. Thus, a relatively small interfacial zone between the two feeds will be formed. This means that there will be a limited area of contact to allow reaction and/or diffusion to occur. Meanwhile, with MM2, where the viscosities of both feeds were similar, it is proposed that the REX mixing will produce a flow containing smaller domains of both NCO and OH and the ''flow'' will contain both NCO and OH reagents. This results in an intermediate reaction zone size and so a larger reaction/diffusion zone will be created. Lastly, the scenario where the NCO feed viscosity is below that of the OH feed and both feed viscosities are significantly lower than that of the NCO feed gives rise to MM1 behaviour. This MM will produce very small domains of OH feed that now are essentially present in a ''flow'' of NCO reagent mixture. This smaller domain morphology was attributed to the lower viscosities of these feeds resulting in greater mixing efficiency and so a significantly larger reaction interface will be created. This hypothesis is supported by the observations on yield stresses and elasticity of the two feeds. Higher yield stresses were exhibited by the NCO feeds when compared to the OH ink with the same level of FS loading. Potentially this arises because of

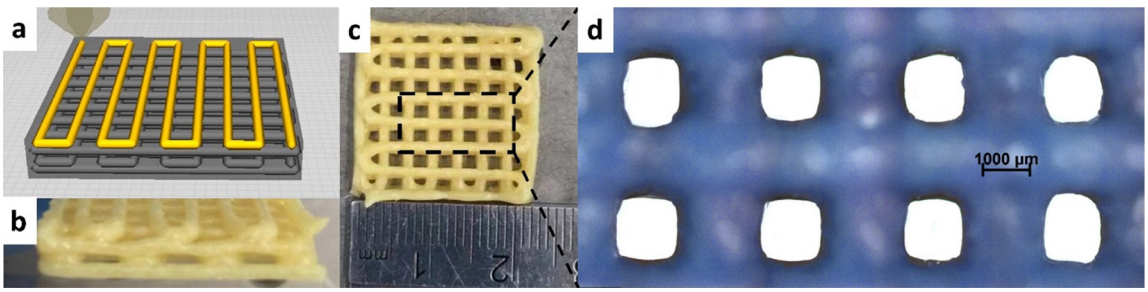


Fig. 6 Woodpile feature blocks printed using the investigated PU formulation MM3. (a) Design pattern, (b) front-view, and (c) top-view of the printed structure and (d) microscopic images of the printed structure.

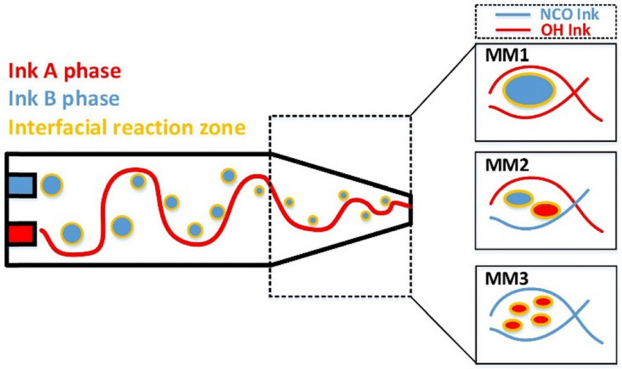


Fig. 7 Hypothesized format of MM domains achieved with different feed properties.

better interaction/wetting between the FS particles with the NCO matrix materials. This supported the proposal that this feed would be harder to break into smaller domains, thus would adopt MM1 type behaviour when compared to the other formulations. Additionally, the elasticity ratio (Fig. 1b) for MM3 (80.04) was found to be four orders of magnitude higher than that of MM1 (0.06). Meanwhile, the viscosity ratio increase was a single order of magnitude by comparison. The greater the difference between these two parameters then the more likely the system is to favour the deformation of the dispersed phase into smaller domains.[54] This will result in a larger interfacial reaction/diffusion zone between the two phases. Thus, MM1 is believed to be the most hindered by reaction/diffusion limitations with the smallest interfacial reaction zone among the three MMs. Furthermore, whilst more study is required to define if the proposed material domains are produced by the different mixing modes are a true reflection of the inner structure of the reacting bead, this suggests that thermal post-processing may not always result in material property improvement when reactants are not intimately mixed.

## Conclusions

This manuscript reports a rigorous study of the reactive extrusion (REX) processing of multi-material, polyurethane-silica composite formulations. This work clearly demonstrated that variations in the mixing modes arising from differences in the relative viscosities of the dual feeds have a significant impact upon the reaction exotherms observed and the ultimate success of polyurethane-based REX. Furthermore, it demonstrated that a multi-functional poly(isocyanate) reagent, exhibiting low volatility, could be utilised to improve flow process safety and allow the processing to be conducted with only local extraction. Furthermore, by relating feed viscosity to the reaction exotherm achieved and the extent of reaction attained, successful printing of dimensionally accurate and resilient 3-dimensional structures was achieved. Thus, this study highlighted that understanding the level of actual cure that is achieved in these cross-linked thermosets is very important, if high-performance devices are to be produced, even when using multi-functional reagents. The feed characteristics were systematically altered by the introduction of fumed silica particles, and were shown to directly determine the mixing efficiencies achieved. In turn the mixing mode attained determined both the reaction kinetics and final properties of a printed bead. The feed combinations that contained NCO feeds that exhibited similar or lower viscosities compared to that of the OH were identified as the most effective (MM3 mode). This conclusion was supported by the following observations: (a) accelerated reaction kinetics, evidenced by a larger polymerisation exotherm; (b) formation of a stronger cross-linked network evidenced by a final PU with higher thermal decomposition temperature and glass transition temperature values and (c) produced a PU polymer that exhibited improved mechanical properties. These enhancements were attributed to the larger viscosity and elasticity contrast between the two feeds in MM3 mixing, which promoted deformation of the dispersed phase into smaller domains. This, in turn, increased the interfacial reaction and diffusion zone, resulting in superior material properties. The ability to tune REX-printed bead properties by adjusting feed rheology also enabled MM3 to be identified as the most suitable mixing mode for printing multi-layer woodpile structures with good structural integrity. By correlating feed viscosity with the extent of reaction achieved, this study demonstrates the successful printing of dimensionally accurate and mechanically robust three-dimensional structures. The success of the printing campaign was demonstrated by the free-standing overhang of the second layer, which did not bow under gravity, and by the high fidelity of the printed structures to their CAD models, *i.e.* showing less than 6%-dimensional deviation. These findings not only inform future efforts in multi-layer, multi-material REX based PU manufacture but also provide broader insights into improving the design of new reactive 3D printing formulations and fully exploit the advantages of *in situ* reactive 3D printing. Furthermore, it is envisioned that following this guidance on the feed rheology properties, a much wider range of chemistries and particle types could be printed using REX to produce functional multi-material gradient materials by selectively tuning the mixing ratio between the feeds. For example, to replicate the heterogeneous functionalities and anisotropic properties exhibited in the biological materials,[80] and/or to contain particles with surface functionality that would increase the level of reactive surface area and so potentially improve final build materials properties. It also indicated that there is a need to further develop spectroscopic analysis techniques for the thermoset materials to more accurately define the degree of cure achieved.

## Author contributions

Y. Wu: experimental conceptualization, methodology, formal analysis, investigation, writing: original draft. Z. Zhou: supervision, writing: review and editing. X. Lu: experimental conceptualization. A. Stimpson: supervision and polymerization support. A. Forchetti Casarino: writing: review and editing.

C. Tuck: review and editing. W. Hayes: writing: review and editing. D. Irvine, R. Wildman: project conceptualization, supervision, writing: review and editing, project administration, fund acquisition.

## Conflicts of interest

The authors declare no competing financial interests.

## Data availability

The data supporting this article have been included as part of the supplementary information (SI). Supplementary information: Tables S1 and S2, rheological and viscosity data, FTIR spectra, DSC/DMA data, exotherm profiles, apparatus figures and 3D printing details. See DOI: https://doi.org/10.1039/d5ma01460c.

## Acknowledgements

The authors acknowledge funding from the Engineering and Physical Sciences Research Council (EPSRC) *via* research grant EP/N024818/1 entitled ''Formulation for 3D Printing: Creating a Plug and Play Platform for a Disruptive UK Industry'' and program grant EP/P031684/1 entitled ''Enabling Next Generation Additive Manufacturing''.

## References

1 A. J. Capel, R. P. Rimington, M. P. Lewis and S. D. R. Christie, 3D Printing for Chemical, Pharmaceutical and Biological Applications, *Nat. Rev. Chem.*, 2018, **2**(12), 422–436, DOI: 10.1038/s41570-018-0058-y.

2 S. C. Ligon, R. Liska, J. Stampfl, M. Gurr and R. Mülhaupt, Polymers for 3D Printing and Customized Additive Manufacturing, *Chem. Rev.*, 2017, **117**(15), 10212–10290, DOI: 10.1021/acs.chemrev.7b00074.

3 J. O. Akindoyo, M. D. H. Beg, S. Ghazali, M. R. Islam, N. Jeyaratnam and A. R. Yuvaraj, Polyurethane Types, Synthesis and Applications – a Review, *RSC Adv.*, 2016, **6**(115), 114453–114482, DOI: 10.1039/C6RA14525F.

4 H. W. Engels, H. G. Pirkl, R. Albers, R. W. Albach, J. Krause, A. Hoffmann, H. Casselmann and J. Dormish, Polyurethanes: Versatile Materials and Sustainable Problem Solvers for Today's Challenges, *Angew. Chem., Int. Ed.*, 2013, **52**(36), 9422–9441, DOI: 10.1002/anie.201302766.

5 L. Zhang, M. Zhang, L. Hu and Y. Zhou, Synthesis of Rigid Polyurethane Foams with Castor Oil-Based Flame Retardant Polyols, *Ind. Crops Prod.*, 2014, **52**, 380–388, DOI: 10.1016/j.indcrop.2013.10.043.

6 V. V. Gite, P. P. Mahulikar and D. G. Hundiwale, Preparation and Properties of Polyurethane Coatings Based on Acrylic Polyols and Trimer of Isophorone Diisocyanate, *Prog. Org. Coat.*, 2010, **68**(4), 307–312, DOI: 10.1016/j.porgcoat.2010.03.008.

7 H. Sheikhy, M. Shahidzadeh, B. Ramezanzadeh and F. Noroozi, Studying the Effects of Chain Extenders Chemical Structures on the Adhesion and Mechanical Properties of a Polyurethane Adhesive, *J. Ind. Eng. Chem.*, 2013, **19**(6), 1949–1955, DOI: 10.1016/j.jiec.2013.03.008.

8 S. Salimi, Y. Wu, M. I. E. Barreiros, A. A. Natfji, S. Khaled, R. D. Wildman, L. R. Hart, F. Greco, E. A. Clark, C. Roberts and W. Hayes, A 3D Printed Drug Delivery Implant Formed from a Dynamic Supramolecular Polyurethane Formulation, *Polym. Chem.*, 2020, **11**(20), 3453–3464, DOI: 10.1039/d0py00068j.

9 L. H. Sinh, K. Harri, L. Marjo, M. Minna, N. D. Luong, W. Jürgen, W. Torsten, S. Matthias and S. Jukka, Novel Photo-Curable Polyurethane Resin for Stereolithography, *RSC Adv.*, 2016, **6**(56), 50706–50709, DOI: 10.1039/c6ra05045j.

10 S. Yuan, F. Shen, J. Bai, C. K. Chua, J. Wei and K. Zhou, 3D Soft Auxetic Lattice Structures Fabricated by Selective Laser Sintering: TPU Powder Evaluation and Process Optimization, *Mater. Des.*, 2017, **120**, 317–327, DOI: 10.1016/j.matdes.2017.01.098.

11 S. R. G. Bates, I. R. Farrow and R. S. Trask, Compressive Behaviour of 3D Printed Thermoplastic Polyurethane Honeycombs with Graded Densities, *Mater. Des.*, 2019, **162**, 130–142, DOI: 10.1016/j.matdes.2018.11.019.

12 S. R. G. Bates, I. R. Farrow and R. S. Trask, 3D Printed Polyurethane Honeycombs for Repeated Tailored Energy Absorption, *Mater. Des.*, 2016, **112**, 172–183, DOI: 10.1016/j.matdes.2016.08.062.

13 M. Müller, Q. U. Huynh, E. Uhlmann and M. H. Wagner, Study of Inkjet Printing as Additive Manufacturing Process for Gradient Polyurethane Material, *Prod. Eng.*, 2014, **8**(1–2), 25–32, DOI: 10.1007/s11740-013-0504-0.

14 C. Sturgess, C. J. Tuck, I. A. Ashcroft and R. D. Wildman, 3D Reactive Inkjet Printing of Polydimethylsiloxane, *J. Mater. Chem. C*, 2017, **5**(37), 9733–9745, DOI: 10.1039/c7tc02412f.

15 Y. Liu, M. Hildner, O. Roy, W. A. Van Den Bogert, J. Lorenz, M. Desroches, K. Koppi, A. Shih and R. G. Larson, On the Selection of Rheological Tests for the Prediction of 3D Printability, *J. Rheol.*, 2023, **67**(4), 791, DOI: 10.1122/8.0000612.

16 P. Kröber, J. T. Delaney, J. Perelaer and U. S. Schubert, Reactive Inkjet Printing of Polyurethanes, *J. Mater. Chem.*, 2009, **19**(29), 5234–5238, DOI: 10.1039/b823135d.

17 B.-J. de Gans, P. C. Duineveld and U. S. Schubert, Inkjet Printing of Polymers: State of the Art and Future Developments, *Adv. Mater.*, 2004, **16**(3), 203–213, DOI: 10.1002/adma.200300385.

18 L. Ren, Z. Song, H. Liu, Q. Han, C. Zhao, B. Derby, Q. Liu and L. Ren, 3D Printing of Materials with Spatially Non-Linearly Varying Properties, *Mater. Des.*, 2018, **156**, 470–479, DOI: 10.1016/j.matdes.2018.07.012.

19 D. Kokkinis, M. Schaffner and A. R. Studart, Multimaterial Magnetically Assisted 3D Printing of Composite Materials, *Nat. Commun.*, 2015, **6**(1), 8643, DOI: 10.1038/ncomms9643.

20 D. Kokkinis, F. Bouville and A. R. Studart, 3D Printing of Materials with Tunable Failure via Bioinspired Mechanical

 

Gradients, *Adv. Mater.*, 2018, **30**(19), 1705808, DOI: 10.1002/adma.201705808.

21 S. Walker, U. Daalkhaijav, D. Thrush, C. Branyan, O. D. Yirmibesoglu, G. Olson and Y. Menguc, Zero-Support 3D Printing of Thermoset Silicone Via Simultaneous Control of Both Reaction Kinetics and Transient Rheology, *3D Print. Addit. Manuf.*, 2019, **6**(3), 139–147, DOI: 10.1089/3dp.2018.0117.

22 O. D. Yirmibesoglu, J. Morrow, S. Walker, W. Gosrich, R. Canizares, H. Kim, U. Daalkhaijav, C. Fleming, C. Branyan and Y. Menguc, Direct 3D Printing of Silicone Elastomer Soft Robots and Their Performance Comparison with Molded Counterparts, *2018 IEEE Int. Conf. Soft Robot. RoboSoft*, 2018, pp. 295–302, DOI: 10.1109/ROBOSOFT.2018.8404935.

23 D. R. Fenn, K. G. Olson, R. M. Rock, C. Kutchko, S. F. Donaldson, H. Sun, O. Rios and W. Carter, *Methods for Reactive Three-Dimensional Printing by Extrusion*, 2016.

24 O. Rios, W. Carter, B. Post, P. Lloyd, D. Fenn, C. Kutchko, R. Rock, K. Olson and B. Compton, 3D Printing via Ambient Reactive Extrusion, *Mater. Today Commun.*, 2018, **15**, 333–336, DOI: 10.1016/j.mtcomm.2018.02.031.

25 P. Wei, C. Cipriani, C.-M. Hsieh, K. Kamani, S. Rogers and E. Pentzer, Go with the Flow: Rheological Requirements for Direct Ink Write Printability, *J. Appl. Phys.*, 2023, **134**(10), 100701, DOI: 10.1063/5.0155896.

26 H. Vanoene, Modes of Dispersion of Viscoelastic Fluids in Flow, *J. Colloid Interface Sci.*, 1972, **40**(3), 448–467, DOI: 10.1016/0021-9797(72)90355-4.

27 D. A. Rau, M. J. Bortner and C. B. Williams, A Rheology Roadmap for Evaluating the Printability of Material Extrusion Inks, *Addit. Manuf*, 2023, **75**, 103745, DOI: 10.1016/j.addma.2023.103745.

28 Q. Zheng, B. Xie, Z. Xu and H. Wu, A Systematic Printability Study of Direct Ink Writing towards High-Resolution Rapid Manufacturing, *Int. J. Extreme Manuf.*, 2023, **5**(3), 035002, DOI: 10.1088/2631-7990/acd090.

29 O. Uitz, P. Koirala, M. Tehrani and C. C. Seepersad, Fast, Low-Energy Additive Manufacturing of Isotropic Parts via Reactive Extrusion, *Addit. Manuf*, 2021, **41**, 101919, DOI: 10.1016/j.addma.2021.101919.

30 O. Uitz, R. Leng, T. Pan, X. Zhao, A. Oridate, C. Seepersad, Z. Ounaies and M. Frecker, Reactive Extrusion Additive Manufacturing (REAM) of Functionally Graded, Magneto-Active Thermoset Composites, *Addit. Manuf*, 2023, **67**, 103486, DOI: 10.1016/j.addma.2023.103486.

31 H. Song, M. J. Fogg, M. Tehrani and C. Seepersad, Investigating the Effects of Processing Parameters in Reactive Extrusion Additive Manufacturing, *Addit. Manuf*, 2025, **101**, 104716, DOI: 10.1016/j.addma.2025.104716.

32 Isocyanates. Health and Safety Executive, https://www.hseni.gov.uk/articles/isocyanates.

33 Guide to handling isocyanates|Safe Work Australia, https://www.safeworkaustralia.gov.au/doc/guide-handling-isocyanates.

34 Lubricants and Lubrication, 2 Volume Set, 3rd Edition, Wiley. Wiley.com, https://www.wiley.com/en-gb/Lubricants+and+Lubrication%2C+2+Volume+Set%2C+3rd+Edition-p-9783527645565.

35 978-87-93026-91-9.pdf. https://www2.mst.dk/Udgiv/publications/2014/01/978-87-93026-91-9.pdf.

36 Poly(phenyl isocyanate)-co-formaldehyde average $M_n$ 400 9016-87-9. https://www.sigmaaldrich.com/GB/en/product/aldrich/406597?srsltid=AfmBOopVJlO0FIOscS5n5G_OHMG8SU57ALUWWoQJ2IVrW-L4svKdfVPu (accessed 2025-11-13).

37 Q. Chen, P.-F. Cao and R. C. Advincula, Mechanically Robust, Ultraelastic Hierarchical Foam with Tunable Properties via 3D Printing, *Adv. Funct. Mater.*, 2018, **28**(21), 1800631, DOI: 10.1002/adfm.201800631.

38 M. Preghenella, A. Pegoretti and C. Migliaresi, Thermo-Mechanical Characterization of Fumed Silica-Epoxy Nanocomposites, *Polymer*, 2005, **46**(26), 12065–12072, DOI: 10.1016/j.polymer.2005.10.098.

39 G. Mansour and D. Tzetzis, Nanomechanical Characterization of Hybrid Multiwall Carbon Nanotube and Fumed Silica Epoxy Nanocomposites, *Polym.-Plast. Technol. Eng.*, 2013, **52**(10), 1054–1062, DOI: 10.1080/03602559.2013.769581.

40 K. Altaf, I. A. Ashcroft and R. Hague, Investigation of the Effect of Relative Humidity on Polymers by Depth Sensing Indentation, *J. Mater. Sci.*, 2011, **46**(23), 7551–7557, DOI: 10.1007/s10853-011-5729-8.

41 N. S. Hmeidat, J. W. Kemp and B. G. Compton, High-Strength Epoxy Nanocomposites for 3D Printing, *Compos. Sci. Technol.*, 2018, **160**, 9–20, DOI: 10.1016/j.compscitech.2018.03.008.

42 L. von Damnitz and D. Anders, A Review on the Mixing Quality of Static Mixers, *ChemEng*, 2025, **9**(6), 128, DOI: 10.3390/chemengineering9060128.

43 A. Bakker, R. LaRoche and E. Marshall, *Laminar Flow in Static Mixer with Helical Elements*, 1998.

44 P. Wang, D. Auhl, E. Uhlmann, G. Gerlitzky and M. H. Wagner, Rheological and Mechanical Gradient Properties of Polyurethane Elastomers for 3D-Printing with Reactive Additives, *Appl. Rheol.*, 2020, **29**(1), 162–172, DOI: 10.1515/arh-2019-0014.

45 P. K. Behera, K. M. Usha, P. K. Guchhait, D. Jehnichen, A. Das, B. Voit and N. K. Singha, A Novel Ionomeric Polyurethane Elastomer Based on Ionic Liquid as Cross-linker, *RSC Adv.*, 2016, **6**(101), 99404–99413, DOI: 10.1039/c6ra21650a.

46 J. Xu, L. Cheng, Z. Zhang, L. Zhang, C. Xiong, W. Huang, Y. Xie and L. Yang, Highly Exfoliated Montmorillonite Clay Reinforced Thermoplastic Polyurethane Elastomer: In Situ Preparation and Efficient Strengthening, *RSC Adv.*, 2019, **9**(15), 8184–8196, DOI: 10.1039/C8RA10121C.

47 H. Vahabi, F. Laoutid, M. Mehrpouya, M. R. Saeb and P. Dubois, Flame Retardant Polymer Materials: An Update and the Future for 3D Printing Developments, *Mater. Sci. Eng., R*, 2021, **144**, 100604, DOI: 10.1016/j.mser.2020.100604.

48 S. Wu, Formation of Dispersed Phase in Incompatible Polymer Blends: Interfacial and Rheological Effects, *Polym. Eng. Sci.*, 1987, **27**(5), 335–343, DOI: 10.1002/pen.760270506.

49 R. Gonzalez-Nunez, B. D. Favis, P. J. Carreau and C. Lavallée, Factors Influencing the Formation of Elongated Morphologies in Immiscible Polymer Blends during Melt Processing, *Polym. Eng. Sci.*, 1993, **33**(13), 851–859, DOI: 10.1002/pen.760331310.

50 I. S. Miles and A. Zurek, Preparation, Structure, and Properties of Two-phase Co-continuous Polymer Blends, *Polym. Eng. Sci.*, 1988, **28**(12), 796–805, DOI: 10.1002/pen.760281205.

51 R. Cardinaels and P. Moldenaers, Morphology Development in Immiscible Polymer Blends, *Polymer Morphology*, John Wiley & Sons, Ltd, 2016, pp. 348–373, DOI: 10.1002/9781118892756.ch19.

52 P. G. Ghodgaonkar and U. Sundararaj, Prediction of Dispersed Phase Drop Diameter in Polymer Blends: The Effect of Elasticity, *Polym. Eng. Sci.*, 1996, **36**(12), 1656–1665, DOI: 10.1002/pen.10562.

53 R. G. Pearson and E. L. Williams, Interfacial Polymerization of an Isocyanate and a Diol, *J. Polym. Sci.: Polym. Chem. Ed.*, 1985, **23**(1), 9–18, DOI: 10.1002/pol.1985.170230102.

54 V. W. A. Verhoeven, A. D. Padsalgikar, K. J. Ganzeveld and L. P. B. M. Janssen, *The Reactive Extrusion of Thermoplastic Polyurethane and the Effect of the Depolymerization Reaction*, 2006, vol. 21.

55 S. C. Machuga, H. L. Midje, J. S. Peanasky, C. W. Macosko and W. E. Ranz, Microdispersive Interfacial Mixing in Fast Polymerizations, *AIChE J.*, 1988, **34**(7), 1057–1064, DOI: 10.1002/aic.690340702.

56 S. Aparna and M. Chandrasekaran, Enhanced Mechanical Properties and Thermal Characteristics of Silica Nanoparticle-Reinforced Hybrid Polymer Composites for Bio-Medical Applications, *Prog. Eng. Sci.*, 2026, **3**(1), 100224, DOI: 10.1016/j.pes.2026.100224.

57 H. Wang, P. Xu, W. Zhong, L. Shen and Q. Du, Transparent Poly(Methyl Methacrylate)/Silica/Zirconia Nanocomposites with Excellent Thermal Stabilities, *Polym. Degrad. Stab.*, 2005, **87**(2), 319–327, DOI: 10.1016/j.polymdegradstab.2004.08.015.

58 N. Katsikis, F. Zahradnik, A. Helmschrott, H. Münstedt and A. Vital, Thermal Stability of Poly(Methyl Methacrylate)/Silica Nano- and Microcomposites as Investigated by Dynamic-Mechanical Experiments, *Polym. Degrad. Stab.*, 2007, **92**(11), 1966–1976, DOI: 10.1016/j.polymdegradstab.2007.08.009.

59 J. A. Lewis, Direct-Write Assembly of Ceramics from Colloidal Inks, *Curr. Opin. Solid State Mater. Sci.*, 2002, **6**(3), 245–250, DOI: 10.1016/S1359-0286(02)00031-1.

60 E. J. Courtial, C. Perrinet, A. Colly, D. Mariot, J. M. Frances, R. Fulchiron and C. Marquette, Silicone Rheological Behavior Modification for 3D Printing: Evaluation of Yield Stress Impact on Printed Object Properties, *Addit. Manuf*, 2019, **28**, 50–57, DOI: 10.1016/j.addma.2019.04.006.

61 M. H. G. Wichmann, M. Cascione, B. Fiedler, M. Quaresimin and K. Schulte, Influence of Surface Treatment on Mechanical Behaviour of Fumed Silica/Epoxy Resin Nanocomposites, *Compos. Interfaces*, 2006, **13**(8–9), 699–715, DOI: 10.1163/156855406779366723.

62 J. W. Maisel and S. K. Wason, Rheology of Precipitated Silica in epoxies, *Polym.-Plast. Technol. Eng.*, 1982, **19**(2), 227–242, DOI: 10.1080/03602558208067732.

63 M. A. Thorseth, J. D. Harris, J. Gu, J. Cuthbert, L. Huffman, K. Capaldo and Z. Jia, Microscopy of Polyurea Grease, *Microsc. Microanal.*, 2021, **27**(1), 12–19, DOI: 10.1017/S1431927620024794.

64 D. Muller, C. Matta, R. Thijssen, M. N. bin Yusof, M. C. P. van Eijk and S. Chatra, Novel Polymer Grease Microstructure and Its Proposed Lubrication Mechanism in Rolling/Sliding Contacts, *Tribol. Int.*, 2017, **110**, 278–290, DOI: 10.1016/j.triboint.2017.02.030.

65 S. M. Olhero and J. M. F. Ferreira, Influence of Particle Size Distribution on Rheology and Particle Packing of Silica-Based Suspensions, *Powder Technol.*, 2004, **139**(1), 69–75, DOI: 10.1016/j.powtec.2003.10.004.

66 S. K. Romberg, M. Islam, C. J. Hershey, M. DeVinney, C. E. Duty, V. Kunc and B. G. Compton, Linking Thermoset Ink Rheology to the Stability of 3D-Printed Structures, *Addit. Manuf.*, 2020, 101621, DOI: 10.1016/j.addma.2020.101621.

67 C. Tan, T. Tirri and C.-E. Wilen, Investigation on the Influence of Chain Extenders on the Performance of One-Component Moisture-Curable Polyurethane Adhesives, *Polymers*, 2017, **9**(12), 184, DOI: 10.3390/polym9050184.

68 A. Pattanayak and S. C. Jana, Thermoplastic Polyurethane Nanocomposites of Reactive Silicate Clays: Effects of Soft Segments on Properties, *Polymer*, 2005, **46**(14), 5183–5193, DOI: 10.1016/j.polymer.2005.04.035.

69 Y. Chen, S. Zhou, H. Yang and L. Wu, Structure and Properties of Polyurethane/Nanosilica Composites, *J. Appl. Polym. Sci.*, 2005, **95**(5), 1032–1039, DOI: 10.1002/app.21180.

70 Q. Li, Y. Pang, X. Liu, E. Xi, A. Mao and H. Wan, Addition of Polyurethane Foam Waste to Polymeric Diphenyl Methane Diisocyanate to Improve Plywood Binder Performance, *For. Prod. J.*, 2020, **70**(3), 262–267, DOI: 10.13073/FPJ-D-19-00062.

71 A. O. Alawode, F. K. Owofadeju, M. Musah, O. Asafu-Adjaye, Y. Peng and B. Via, Performance of Different Fillers in Polymeric Methylene Diphenyl Diisocyanate (pMDI) Resin*, *For. Prod. J.*, 2022, **72**(s1), 14–21, DOI: 10.13073/FPJ-D-22-00018.

72 D. Pedrazzoli and I. Manas-Zloczower, Understanding Phase Separation and Morphology in Thermoplastic Polyurethanes Nanocomposites, *Polym.*, 2016, **90**, 256–263, DOI: 10.1016/j.polymer.2016.03.022.

73 P. Król and B. Pilch-Pitera, Phase Structure and Thermal Stability of Crosslinked Polyurethane Elastomers Based on Well-Defined Prepolymers, *J. Appl. Polym. Sci.*, 2007, **104**(3), 1464–1474, DOI: 10.1002/app.25011.

74 G. Trovati, E. A. Sanches, S. C. Neto, Y. P. Mascarenhas and G. O. Chierice, Characterization of Polyurethane Resins by FTIR, TGA, and XRD, *J. Appl. Polym. Sci.*, 2010, **115**(1), 263–268, DOI: 10.1002/app.31096.

75 Z. S. Petrović, I. Javni and V. Divjaković, Structure and Physical Properties of Segmented Polyurethane Elastomers Containing Chemical Crosslinks in the Hard Segment,

*J. Polym. Sci., Part B: Polym. Phys.*, 1998, **36**(2), 221–235, DOI: 10.1002/(SICI)1099-0488(19980130)36:2%253C221::AID-POLB3%253E3.0.CO;2-U.

76 V. W. A. Verhoeven, A. D. Padsalgikar, K. J. Ganzeveld and L. P. B. M. Janssen, A Kinetic Investigation of Polyurethane Polymerization for Reactive Extrusion Purposes, *J. Appl. Polym. Sci.*, 2006, **101**(1), 370–382, DOI: 10.1002/app.23848.

77 Q. Guo, P. Zhu, G. Li, J. Wen, T. Wang, D. Lu, R. Sun and C. Wong, Study on the Effects of Interfacial Interaction on the Rheological and Thermal Performance of Silica Nanoparticles Reinforced Epoxy Nanocomposites, *Composites, Part B*, 2017, **116**, 388–397, DOI: 10.1016/j.compositesb.2016.10.081.

78 J. A. Lewis, Direct Ink Writing of 3D Functional Materials, *Adv. Funct. Mater.*, 2006, **16**(17), 2193–2204, DOI: 10.1002/adfm.200600434.

79 L. Wang, S. Zhang, Q. Wang, J. Chen, W. Jiang and R. T. Chen, Fabrication of Three-Dimensional (3D) Woodpile Structure Photonic Crystal with Layer by Layer e-Beam Lithography, *Appl. Phys. A: Mater. Sci. Process.*, 2009, **95**(2), 329–334, DOI: 10.1007/s00339-009-5076-7.

80 S. E. Bakarich, R. Gorkin, R. Gately, S. Naficy, M. in het Panhuis and G. M. Spinks, 3D Printing of Tough Hydrogel Composites with Spatially Varying Materials Properties, *Addit. Manuf.*, 2017, **14**, 24–30, DOI: 10.1016/j.addma.2016.12.003.